

T-matrix calculation via Discrete-dipole approximation and exploiting mirror symmetry

Vincent L. Y. Loke,* Timo A. Nieminen, N. R. Heckenberg, and Halina Rubinsztein-Dunlop
School of Physical Sciences, The University of Queensland, Brisbane, Queensland 4072, Australia.

(Dated: October 26, 2021)

We present three methods for calculating the T-matrix for modeling arbitrarily shaped micro-sized objects. When applied to microrotors, their rotation and mirror symmetry can be exploited to reduce memory usage and calculation time by 2 orders of magnitude. In the methods where the T-matrix elements are calculated using point matching with vector spherical fields, mode redundancy can be exploited to reduce calculation time.

PACS numbers: Valid PACS appear here

I. INTRODUCTION

- Motivation: optical rotors
- DDA [? ?]
- Memory requirements of the A matrix, swapping
- Compressed A matrix
- T-matrix [?]
- DDA T-matrix [?]

Our T-matrix methods are

- near VSWF field point matching with DDA field
- far VSWF field point matching with DDA field
- rotate [?] and translate [?]

II. OPTIMIZING THE DISCRETE DIPOLE APPROXIMATION INTERACTION MATRIX

The size of the microdevices we model may exceed 10–20 wavelengths in size, which may well require computational time in excess of several days and RAM beyond that available. To circumvent these limitations, we exploit the discrete rotational and/or mirror symmetry of a microcomponent. This is closely tied with the link between DDA and the T -matrix method. In the T -matrix method, the fields are represented as sums of vector spherical wavefunctions (VSWFs) [? ?], and to use DDA to calculate a T -matrix, we can simply calculate the scattered field (and its VSWF representation) for each possible incident single-mode VSWF field in turn. The important point is that each VSWF is characterized by a simple azimuthal dependence of $\exp(im\phi)$, where m is the azimuthal mode index. If we consider a group of dipoles that are rotationally symmetric about the vertical

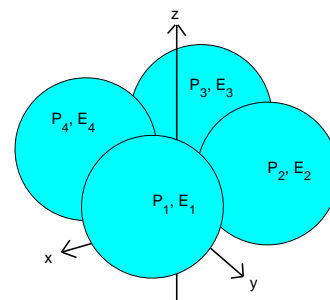


FIG. 1:

axis—in the case of figure 1, there is 4th-order rotational symmetry—the magnitude of the incident field will be the same, the field differing by the vector rotation ϕ and phase factor of $\exp(im\phi)$; only the dipole moment of one repeating unit of the total number of dipoles needs to be known. In spherical coordinates,

$$\vec{P}_q^{sph} = \vec{P}_1^{sph} \exp(im\phi_q). \quad (1)$$

However, our implementation of the interaction matrix [?], electric field and dipole moments were in cartesian coordinates system (what was the advantage?). This requires a transformation of the dipole moment at the first segment from the cartesian to spherical coordinate system followed by a transformation back from spherical to cartesian at the rotational counterpart dipole,

$$\vec{P}_q^{cart} = C_q S \vec{P}_1^{cart} \exp(im\phi_q), \quad (2)$$

where

$$S = \begin{bmatrix} \sin(\theta)\cos(\phi_1) & \sin(\theta)\sin(\phi_1) & \cos(\theta) \\ \cos(\theta)\cos(\phi_1) & \cos(\theta)\sin(\phi_1) & -\sin(\theta) \\ -\sin(\phi_1) & \cos(\phi_1) & 0 \end{bmatrix} \quad (3)$$

is an orthogonal matrix that transforms the \vec{P}_1^{cart} vector into the spherical coordinate system and

$$C_q = \begin{bmatrix} \sin(\theta)\cos(\phi_q) & \sin(\theta)\sin(\phi_q) & \cos(\theta) \\ \cos(\theta)\cos(\phi_q) & \cos(\theta)\sin(\phi_q) & -\sin(\theta) \\ -\sin(\phi_q) & \cos(\phi_q) & 0 \end{bmatrix}^{-1} \quad (4)$$

*Electronic address: loke@physics.uq.edu.au

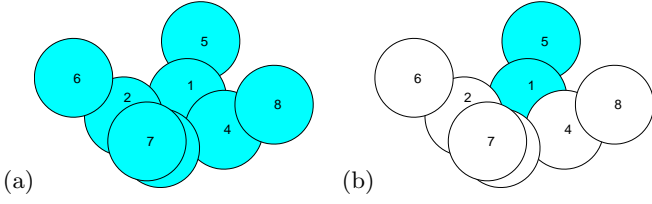


FIG. 2: (a) 8-dipole example. (b) The 2 dipoles required to completely specify all dipole moments.

is a transpose of S but at the azimuthal coordinate of the rotational counterpart dipole.

This brings up question of how to reduce the number of equations such that only one rotational unit needs to be solved. Conventionally, the interaction matrix as defined in [?] represents the coupling between each dipole with all other dipoles. Figure 3(a) shows the interaction matrix for the example set of dipoles shown in figure 2(a). In general the matrix will be made up of $N \times N$ cells for N dipoles; each cell is a 3×3 tensor. In the example, the matrix is made up of 8×8 cells. A diagonal cell represents the self interaction (or the inverse of the polarizability) and an off-diagonal cell represents the coupling between different dipoles. Taking advantage of the equal amplitudes and known phase factors between a dipole and its rotational counterparts, we can reduce the interaction matrix. Taking the example in figure 2(b), we construct the interaction matrix as if there were only 2 dipoles but we aggregate the contribution from the appropriate dipoles. For the off-diagonal cells, the coupling between a dipole with the other dipoles including their rotational counterparts are summed as follows

$$\begin{aligned} \bar{A}_{jk} = & \sum_{q=1}^Q \frac{\exp(ikr_{jk}^{(q)})}{r_{jk}^{(q)}} \\ & \times \left[k^2 (\hat{r}_{jk}^{(q)} \hat{r}_{jk}^{(q)} - I_3) + \frac{ikr_{jk}^{(q)} - 1}{r_{jk}^{2(q)}} (3\hat{r}_{jk}^{(q)} \hat{r}_{jk}^{(q)} - I_3) \right] \\ & \times C_q S \exp(im\phi), \quad j \neq k, \end{aligned} \quad (5)$$

where Q is the order of discrete rotational symmetry, m is the azimuthal mode of the incident VSWF field, q is the rotational segment number, the rotational angle $\phi = 2\pi q/Q$, $r_{jk}^{(q)}$ is the distance from points r_j to the rotationally symmetric points $r_k^{(q)}$, and $\hat{r}_{jk}^{(q)}$ is the unit vector from points r_j to $r_k^{(q)}$. The coordinate for a given rotational symmetric point is calculated using a rotation about the z-axis,

$$r_k^{(q)} = \begin{bmatrix} \cos(q\phi) & -\sin(q\phi) & 0 \\ \sin(q\phi) & \cos(q\phi) & 0 \\ 0 & 0 & 1 \end{bmatrix} r_k. \quad (6)$$

For the diagonal cells, the ‘‘self interaction’’ includes the coupling between a dipole and its rotational counter-

parts:

$$\begin{aligned} \bar{A}_{jj} = & \alpha_j^{-1} + \sum_{q=2}^Q \frac{\exp(ikr_{jk}^{(q)})}{r_{jk}^{(q)}} \\ & \times \left[k^2 (\hat{r}_{jk}^{(q)} \hat{r}_{jk}^{(q)} - I_3) + \frac{ikr_{jk}^{(q)} - 1}{r_{jk}^{2(q)}} (3\hat{r}_{jk}^{(q)} \hat{r}_{jk}^{(q)} - I_3) \right] \\ & \times C_q S \exp(im\phi), \quad j = k. \end{aligned} \quad (7)$$

Figure 3(b) shows the interaction matrix representation for the example dipole system in figure 2(c). The compressed interaction matrix is a factor of Q^2 smaller than the conventional matrix. Having precalculated the inci-

α^{-1}	A	A	A	A	A	A	A
α^{-1}	1,2	1,3	1,4	1,5	1,6	1,7	1,8
A	α^{-1}	A	A	A	A	A	A
2,1	α^{-1}	2,3	2,4	2,5	2,6	2,7	2,8
A	A	α^{-1}	A	A	A	A	A
3,1	3,2	α^{-1}	3,4	3,5	3,6	3,7	3,8
A	A	A	α^{-1}	A	A	A	A
4,1	4,2	4,3	α^{-1}	4,5	4,6	4,7	4,8
A	A	A	A	α^{-1}	A	A	A
5,1	5,2	5,3	5,4	α^{-1}	5,6	5,7	5,8
A	A	A	A	A	α^{-1}	A	A
6,1	6,2	6,3	6,4	6,5	α^{-1}	6,7	6,8
A	A	A	A	A	A	α^{-1}	A
7,1	7,2	7,3	7,4	7,5	7,6	α^{-1}	7,8
A	A	A	A	A	A	A	α^{-1}
8,1	8,2	8,3	8,4	8,5	8,6	8,7	α^{-1}

A	A
1, 2-3-4	1, 5-6-7-8
A	A
5, 1-2-3-4	5, 6-7-8

FIG. 3: (a) Full interaction matrix. (b) Symmetry reduced interaction matrix

dent fields $\vec{E}_{j,inc}$ at each dipole of the rotational unit, we solve for the dipole moments \vec{P}_j for the dipoles with a reduced set of linear equations. The dipole moments and fields of the rotational counterpart dipoles can be calculated by applying the rotational matrix α and phase factor $\exp(im\phi)$.

We can exploit mirror symmetry in a similar fashion, since the VSWFs possess either even or odd parity w.r.t. the xy -plane. This allows a reduction in size by a further factor of 4.

III. METHODS FOR CALCULATING THE T-MATRIX

A. Near field point matching

- vswf field matched with DDA field
- solve for p’s and q’s
- contract T-matrix column by column

$$p_{nm} = \vec{M}_{nm}^{(1)}(kr) / \vec{E}_{DDA,TE_{nm}}, \quad (8)$$

$$q_{nm} = \vec{N}_{nm}^{(1)}(kr) / \vec{E}_{DDA,TM_{nm}} \quad (9)$$

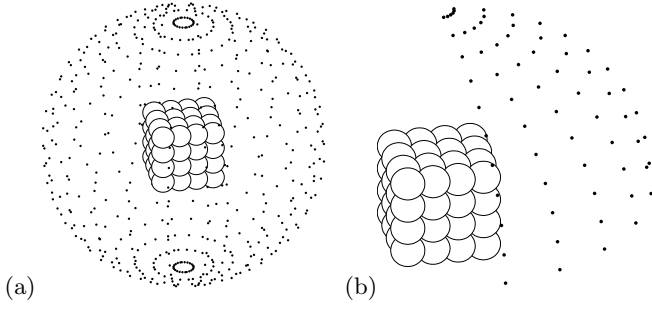


FIG. 4: (a) Near field matching. (b) Octant near field matching.

B. Far field matching

- DDA farfield
- VSH farfield
- solving for p_{nm} and q_{nm}
- Constructing the T-matrix

Far field matching

$$\vec{M}_{nm}^{(1,2)}(kr) = \frac{N_n}{kr} (\mp i)^{n+1} \exp(\pm ikr) \vec{C}_{nm}(\theta, \phi) \quad (10)$$

$$\vec{N}_{nm}^{(1,2)}(kr) = \frac{N_n}{kr} (\mp i)^{n+1} \exp(\pm ikr) \vec{B}_{nm}(\theta, \phi) \quad (11)$$

$$kr \vec{E}(\theta, \phi) = \sum_{nm} a_{nm} \vec{B}_{nm} + b_{nm} \vec{C}_{nm} + c_{nm} \vec{P}_{nm} \quad (12)$$

$$p_{nm} N_n (-i)^{n+1} = b_{nm}, \quad (13)$$

$$q_{nm} N_n (i)^n = a_{nm} \quad (14)$$

$$p_{nm} = \frac{b_{nm}}{N_n (-i)^{n+1}}, \quad (15)$$

$$q_{nm} = \frac{a_{nm}}{N_n (i)^n} \quad (16)$$

C. Rotation and translation of vector fields

- Videen translations [?], precalculated
- Rotations of axes
- Constructing the T-matrix, cycle through m's and n's

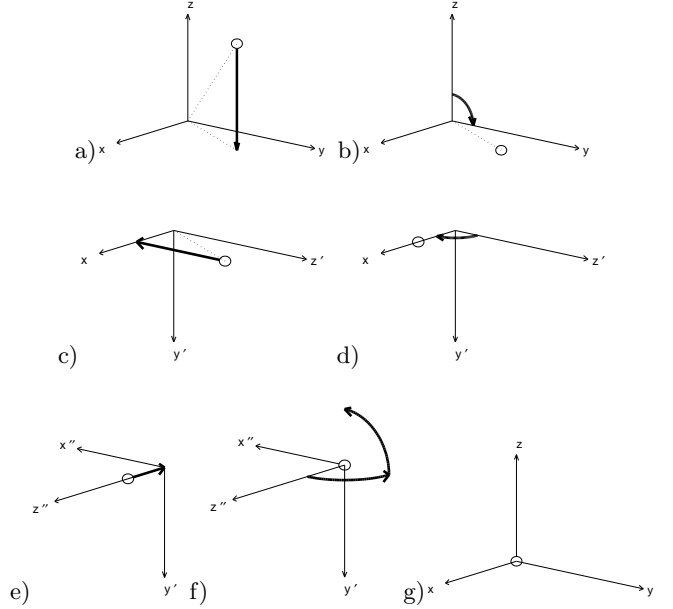


FIG. 5: a) $z = 0$ translation b) z onto y axis rotation c) $z' = 0$ translation d) z' onto x axis rotation e) $z'' = 0$ translation f) rotations back onto the original z -axis g) original orientation

IV. MODE REDUNDANCY AND THE ORDER OF DISCRETE ROTATIONAL SYMMETRY

- Motivation, computational savings
- Explain m th order discrete rotational symmetry and VSWF m modes
- redundant modes
- Floquet's theorem
- $m_{\text{scat}} = m_{\text{inc}} + ip$ (5)
- For a cube, $p = 4$, and $m_{\text{scat}} = m_{\text{inc}}, m_{\text{inc}} + 4, m_{\text{inc}} + 8, \dots$
- time saving

V. RESULTS

A. Phase functions for the spheres and cubes

comparison

- Sphere Mie soln
- cube point matching [?] (toolbox)
- also Wriedt [?]

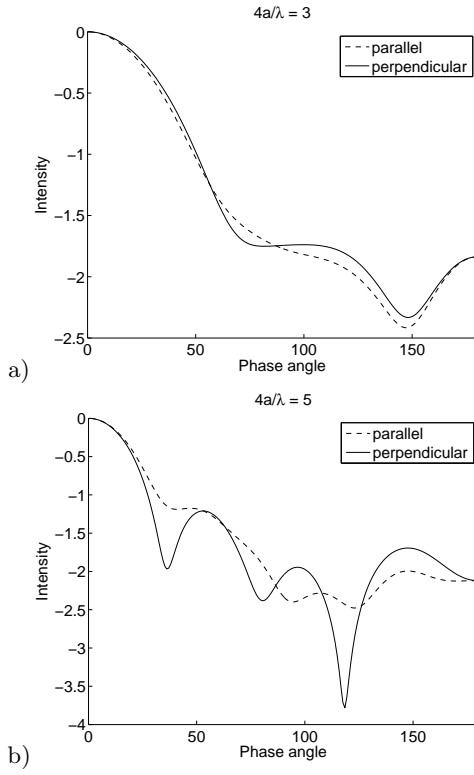


FIG. 6: The phase function for cubes with the refractive index of 1.5 and widths of a) 0.75λ b) 1.25λ .

B. Cross rotor torque calculations

- convergence of torque
- low nrel so $\lambda/5$ suffices
- reference Theo's results

VI. CONCLUSION

Combination of optimization techniques

- DDA rotational and mirror symm, interaction matrix compression
- Far field and near field matrix, octant matching grid points
- exploiting mode redundancy

T -matrix calculation via discrete-dipole approximation, point matching and exploiting symmetry

Vincent L. Y. Loke, Timo A. Nieminen, N. R. Heckenberg, Halina
Rubinsztein-Dunlop

*Centre for Biophotonics and Laser Science, School of Physical Sciences, The University
of Queensland, Brisbane, Queensland 4072, Australia.*

Abstract

We present a method of incorporating the discrete dipole approximation (DDA) method with the point matching method to formulate the T -matrix for modeling arbitrarily shaped micro-sized objects. The T -matrix elements are calculated using point matching between fields calculated using vector spherical wave functions and DDA. When applied to microrotors, their discrete rotational and mirror symmetries can be exploited to reduce memory usage and calculation time by orders of magnitude; a number of optimization methods can be employed based on the knowledge of the relationship between the azimuthal mode and phase at each discrete rotational point, and mode redundancy from Floquet's theorem. A 'reduced-mode' T -matrix can also be calculated if the illumination conditions are known.

Key words: DDA, T -matrix, discrete rotational symmetry, point matching

1. Introduction

Optical tweezers [1] can be used to exert forces and torques and thus drive micromachines [2, 3]. This opens up a new field of micro engineering, whose potential has yet to be fully realized. To aid in designing micromachines, we employ a number of modelling methods ranging from the generalized Lorenz-Mie theory (GLMT) [4], the FDFD/ T -matrix hybrid method [5] to the discrete dipole approximation (DDA) [6, 7]. We use the abovementioned

Email address: loke@physics.uq.edu.au (Vincent L. Y. Loke)

methods to formulate the T -matrix because repeated calculations with different illumination conditions are required. The extended boundary condition method (EBCM) [8, 9] is most commonly used to calculate the T -matrix; however, numerical problems are encountered with high aspect ratio structures [10].

Given the structure of typical optical micromachines [11], we have found the DDA method most suitable. In DDA, the scattering object is represented as a collection of dipole scatterers, and the total scattering problem, including the coupling between the dipoles, is solved. DDA is well-suited to modelling optical micromachines. Firstly, only the volume of the actual particle needs to be discretized, while both the particle and surrounding medium in a volume enclosing the particle are discretized in other general methods such as the finite-difference time-domain method (FDTD) and finite element methods (FEM). Considering that structures as shown in figure 1a are not unusual, where the particle occupies only a relatively small fraction of the nearby volume, this can mean a considerable saving in required memory and time. Secondly, DDA performs well for relatively low contrast scatterers, which is typical of most optical micromachines so far, usually constructed from a polymer material [12] and deployed in a dielectric liquid. Thirdly, it is relatively simple to obtain the T -matrix via DDA if repeated calculations are desired [13]. Finally, it is possible to exploit discrete rotational symmetry of a particle to reduce the computational resources, including both time and memory, by orders of magnitude. This last factor is important, since optical micromachines are often large in overall dimension compared to the wavelength (while having wavelength scale features forcing the use of electromagnetic theory rather than geometric optics), and the available resources can place such devices beyond practical calculation [14]. Figure 1 shows a typical case.

By itself, the DDA method does not give us the T -matrix. One method of formulating the T -matrix via DDA [13] is to transform the field contributions of each dipole to aggregate their contributions at a common origin. We embarked on a different method — incorporated the DDA with the point matching method; both the near and far-field point matching methods are discussed in this paper but only the results of the former are presented. We will also discuss the optimization methods employed.

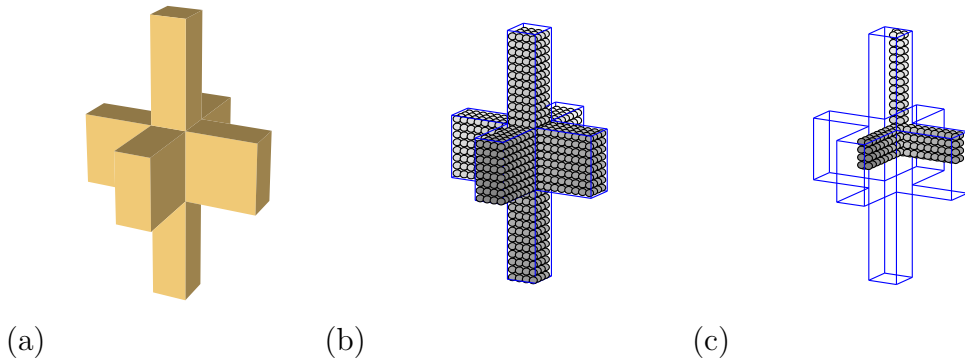


Figure 1: (a) An optically-driven microrotor. (b) Discrete dipole representation of the rotor. (c) Discrete rotational and mirror symmetries allow the modelling of only the repeated segment, with a major reduction in required memory and time.

2. DDA revisited

With DDA, the microrotor in figure 1a can be represented by a set of dipoles in a cubic lattice, as in figure 1b, fashioned to approximate the target structure. The lattice spacing has to be sufficiently small, not only to accurately represent the structure — stair-casing becomes a problem for curved surfaces — but small enough compared to the wavelength of the incident light; the criterion is specified in [7].

We first have to calculate the incident field, $\mathbf{E}_{inc,j}$, at each dipole and the interaction matrix [7]

$$\mathbf{A}_{jk} = \frac{\exp(ikr_{jk})}{r_{jk}} \left[k^2(\hat{r}_{jk}\hat{r}_{jk} - \mathbf{1}_3) + \frac{ikr_{jk} - 1}{r_{jk}^2}(3\hat{r}_{jk}\hat{r}_{jk} - \mathbf{1}_3) \right], \quad j \neq k, \quad (1)$$

where r_{jk} is the distance from points r_j to r_k , \hat{r}_{jk} is the unit vector from in the direction from points r_j to r_k , and

$$\mathbf{A}_{jj} = \alpha_j^{-1} \quad (2)$$

where α_j is the polarizability [15] of each dipole. Equation (1) represents the coupling between the dipoles and (2) allows the system of equations to be written in the compact form

$$\sum_{k=1}^N \mathbf{A}_{jk} \mathbf{P}_j = \mathbf{E}_{inc,j}. \quad (3)$$

since the dipole moment due to the total field at each dipole is $\mathbf{P}_j = \alpha_j \mathbf{E}_j$. Because \mathbf{A}_{jk} is a square matrix, the dipole moments can rapidly solved using the generalized minimum residual method [16].

3. Optimizing the Discrete Dipole Approximation interaction matrix

The size of the microdevices we model may exceed 10–20 wavelengths in size, which may well require computational time in excess of several days and RAM beyond that available. To circumvent these limitations, we exploit the discrete rotational and/or mirror symmetry of a microcomponent. This is closely tied with the link between DDA and the T -matrix method. In the T -matrix method, the fields are represented as sums of vector spherical wavefunctions (VSWFs) [9, 17], and to use DDA to calculate a T -matrix, we can simply calculate the scattered field (and its VSWF representation) for each possible incident single-mode VSWF field in turn. The important point is that each VSWF is characterized by a simple azimuthal dependence of $\exp(im\phi)$, where m is the azimuthal mode index. If we consider a group of

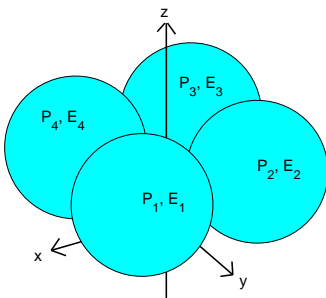


Figure 2: Dipoles in a 4-fold discrete rotationally symmetric arrangement about beam axis.

dipoles that are rotationally symmetric about the vertical axis—in the case of figure 2, there is 4th-order rotational symmetry—the magnitude of the incident field will be the same, the field differing by the vector rotation (9) and phase factor of $\exp(im\phi)$; only the dipole moment of one repeating unit of the total number of dipoles needs to be known. In spherical coordinates,

$$\mathbf{P}_q^{sph} = \mathbf{P}_1^{sph} \exp(im\phi_q). \quad (4)$$

However, our implementation of the interaction matrix[7], electric field and dipole moments were in cartesian coordinates system. This requires a transformation of the dipole moment at the first segment from the cartesian to spherical coordinate system followed by a transformation back from spherical to cartesian at the rotational counterpart dipole,

$$\mathbf{P}_q^{cart} = \mathbf{C}_q \mathbf{S} \mathbf{P}_1^{cart} \exp(im\phi_q), \quad (5)$$

where

$$\mathbf{S} = \begin{bmatrix} \sin(\theta) \cos(\phi_1) & \sin(\theta) \sin(\phi_1) & \cos(\theta) \\ \cos(\theta) \cos(\phi_1) & \cos(\theta) \sin(\phi_1) & -\sin(\theta) \\ -\sin(\phi_1) & \cos(\phi_1) & 0 \end{bmatrix} \quad (6)$$

is an orthogonal matrix that transforms the \mathbf{P}_1^{cart} vector into the spherical coordinate system and

$$\mathbf{C}_q = \begin{bmatrix} \sin(\theta) \cos(\phi_q) & \sin(\theta) \sin(\phi_q) & \cos(\theta) \\ \cos(\theta) \cos(\phi_q) & \cos(\theta) \sin(\phi_q) & -\sin(\theta) \\ -\sin(\phi_q) & \cos(\phi_q) & 0 \end{bmatrix}^{-1} \quad (7)$$

is a transpose of \mathbf{S} but at the azimuthal coordinate of the rotational counterpart dipole. The same transformations and phase corrections are applied to the \mathbf{E} and \mathbf{H} fields. Conventionally, the interaction matrix as defined in

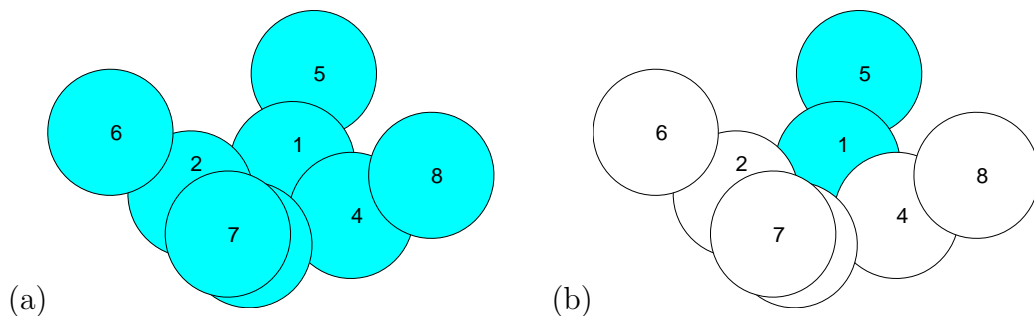


Figure 3: (a) 8-dipole example. (b) The 2 dipoles required to completely specify all dipole moments.

[7] represents the coupling between each dipole with all other dipoles. Figure 4(a) shows the interaction matrix for the example set of dipoles shown in figure 3(a). In general the matrix will be made up of $N \times N$ cells for N dipoles; each cell is a 3×3 tensor. In the example, the matrix is made

up of 8×8 cells. A diagonal cell represents the self interaction (or the inverse of the polarizability) and an off-diagonal cell represents the coupling between different dipoles. Taking advantage of the equal amplitudes and known phase factors between a dipole and its rotational counterparts, we can reduce the interaction matrix. Taking the example in figure 3(b), we construct the interaction matrix as if there were only 2 dipoles but we aggregate the contribution from the appropriate dipoles. For the off-diagonal cells, the coupling between a dipole with the other dipoles including their rotational counterparts are summed as follows

$$\begin{aligned} \mathbf{A}_{jk} &= \sum_{q=1}^Q \frac{\exp(ikr_{jk}^{(q)})}{r_{jk}^{(q)}} \\ &\times \left[k^2(\hat{r}_{jk}^{(q)}\hat{r}_{jk}^{(q)} - \mathbf{1}_3) + \frac{ikr_{jk}^{(q)} - 1}{r_{jk}^{2(q)}}(3\hat{r}_{jk}^{(q)}\hat{r}_{jk}^{(q)} - \mathbf{1}_3) \right] \\ &\times \mathbf{C}_q \mathbf{S} \exp(im\phi), \quad j \neq k, \end{aligned} \quad (8)$$

where Q is the order of discrete rotational symmetry, m is the azimuthal mode of the incident VSWF field, q is the rotational segment number, the rotational angle $\phi = 2\pi q/Q$, $r_{jk}^{(q)}$ is the distance from points r_j to the rotationally symmetric points $r_k^{(q)}$, and $\hat{r}_{jk}^{(q)}$ is the unit vector from points r_j to $r_k^{(q)}$. The coordinate for a given rotational symmetric point is calculated using a rotation about the z-axis,

$$r_k^{(q)} = \begin{bmatrix} \cos(q\phi) & -\sin(q\phi) & 0 \\ \sin(q\phi) & \cos(q\phi) & 0 \\ 0 & 0 & 1 \end{bmatrix} r_k. \quad (9)$$

For the diagonal cells, the ‘‘self interaction’’ includes the coupling between a dipole and its rotational counterparts:

$$\begin{aligned} \mathbf{A}_{jj} &= \alpha_j^{-1} + \sum_{q=2}^Q \frac{\exp(ikr_{jk}^{(q)})}{r_{jk}^{(q)}} \\ &\times \left[k^2(\hat{r}_{jk}^{(q)}\hat{r}_{jk}^{(q)} - \mathbf{1}_3) + \frac{ikr_{jk}^{(q)} - 1}{r_{jk}^{2(q)}}(3\hat{r}_{jk}^{(q)}\hat{r}_{jk}^{(q)} - \mathbf{1}_3) \right] \\ &\times \mathbf{C}_q \mathbf{S} \exp(im\phi), \quad j = k. \end{aligned} \quad (10)$$

Figure 4(b) shows the interaction matrix representation for the example dipole system in figure 3(c). The compressed interaction matrix is a factor of Q^2 smaller than the conventional matrix. Having precalculated the

α^{-1}	α^{-1}	α^{-1}	α^{-1}	α^{-1}	α^{-1}	α^{-1}	α^{-1}
\mathbf{A}	\mathbf{A}	\mathbf{A}	\mathbf{A}	\mathbf{A}	\mathbf{A}	\mathbf{A}	\mathbf{A}
1, 2	1, 3	1, 4	1, 5	1, 6	1, 7	1, 8	
\mathbf{A}	α^{-1}	α^{-1}	α^{-1}	α^{-1}	α^{-1}	α^{-1}	α^{-1}
2, 1	α^{-1}	2, 3	2, 4	2, 5	2, 6	2, 7	2, 8
\mathbf{A}	\mathbf{A}	α^{-1}	α^{-1}	α^{-1}	α^{-1}	α^{-1}	α^{-1}
3, 1	3, 2	α^{-1}	3, 4	3, 5	3, 6	3, 7	3, 8
\mathbf{A}	\mathbf{A}	\mathbf{A}	α^{-1}	α^{-1}	α^{-1}	α^{-1}	α^{-1}
4, 1	4, 2	4, 3	α^{-1}	4, 5	4, 6	4, 7	4, 8
\mathbf{A}	\mathbf{A}	\mathbf{A}	\mathbf{A}	α^{-1}	α^{-1}	α^{-1}	α^{-1}
5, 1	5, 2	5, 3	5, 4	α^{-1}	5, 6	5, 7	5, 8
\mathbf{A}	\mathbf{A}	\mathbf{A}	\mathbf{A}	\mathbf{A}	α^{-1}	α^{-1}	α^{-1}
6, 1	6, 2	6, 3	6, 4	6, 5	α^{-1}	6, 7	6, 8
\mathbf{A}	\mathbf{A}	\mathbf{A}	\mathbf{A}	\mathbf{A}	\mathbf{A}	α^{-1}	α^{-1}
7, 1	7, 2	7, 3	7, 4	7, 5	7, 6	α^{-1}	7, 8
\mathbf{A}	\mathbf{A}	\mathbf{A}	\mathbf{A}	\mathbf{A}	\mathbf{A}	\mathbf{A}	α^{-1}
8, 1	8, 2	8, 3	8, 4	8, 5	8, 6	8, 7	α^{-1}

\mathbf{A}	\mathbf{A}
1, 2-3-4	1, 5-6-7-8
\mathbf{A}	\mathbf{A}
5, 1-2-3-4	5, 6-7-8

Figure 4: (a) Full interaction matrix. (b) Compressed interaction matrix.

incident fields $\mathbf{E}_{j,inc}$ at each dipole of the rotational unit, we solve for the dipole moments \mathbf{P}_j for the dipoles with a reduced set of linear equations:

$$\sum_{k=1}^N \mathbf{A}_{quad,jk}(m) \mathbf{P}_{quad,j} = \mathbf{E}_{inc,quad,j}. \quad (11)$$

Notice that the discrete rotationally optimized A-matrix is m dependent; the A-matrices can be precalculated and loaded as cycle the required azimuthal modes (m) of the incident beam. However, there is some degree of redundancy; e.g., when m is even, $\mathbf{A}(m) = \mathbf{A}(-m)$. The dipole moments of the rotational counterpart dipoles can be calculated by applying the rotational matrix 9 and phase factor $\exp(im\phi)$.

We can exploit mirror symmetry in a similar fashion, since a VSWF possess either even or odd parity with respect to the the xy -plane. In the

Cartesian coordinate system, when $n + m$ is odd,

$$\begin{aligned} \mathbf{P}_{TE}^{(+x)} &= \mathbf{P}_{TE}^{(-x)}, \mathbf{P}_{TE}^{(+y)} = \mathbf{P}_{TE}^{(-y)}, \mathbf{P}_{TE}^{(+z)} = -\mathbf{P}_{TE}^{(-z)} \\ \mathbf{P}_{TM}^{(+x)} &= -\mathbf{P}_{TM}^{(-x)}, \mathbf{P}_{TM}^{(+y)} = -\mathbf{P}_{TM}^{(-y)}, \mathbf{P}_{TM}^{(+z)} = \mathbf{P}_{TM}^{(-z)}, \end{aligned} \quad (12)$$

and when $n + m$ is even,

$$\begin{aligned} \mathbf{P}_{TE}^{(+x)} &= -\mathbf{P}_{TE}^{(-x)}, \mathbf{P}_{TE}^{(+y)} = -\mathbf{P}_{TE}^{(-y)}, \mathbf{P}_{TE}^{(+z)} = \mathbf{P}_{TE}^{(-z)} \\ \mathbf{P}_{TM}^{(+x)} &= \mathbf{P}_{TM}^{(-x)}, \mathbf{P}_{TM}^{(+y)} = \mathbf{P}_{TM}^{(-y)}, \mathbf{P}_{TM}^{(+z)} = -\mathbf{P}_{TM}^{(-z)}. \end{aligned} \quad (13)$$

This allows a reduction in size of the A-matrix by a further factor of 4.

4. The incident beam

The optical tweezers that are used to drive micromachines are usually tightly focused laser beams. The beams may be linearly or circularly polarized (has spin angular momentum), and may or may not carry orbital angular momentum. For example, we use an LG_{02} beam, which carries orbital angular momentum of $2\hbar$ per photon, to trap and rotate the microrotors such as the one in figure 1a.

We calculate the incident field at each dipole using the vector spherical wave function expansion (VSWF)

$$\mathbf{E}_{\text{inc}} = \sum_{n=1}^{\infty} \sum_{m=-n}^n a_{nm} \mathbf{M}_{nm}^{(3)}(kr) + b_{nm} \mathbf{N}_{nm}^{(3)}(kr), \quad (14)$$

where k is the wave vector, r is the dipole position in spherical coordinates, n is the radial mode index, m is the azimuthal mode index and $\mathbf{M}_{nm}^{(3)}$ & $\mathbf{N}_{nm}^{(3)}$ are regular VSWFs [18, 19]; a_{nm} and b_{nm} are incident coefficients for the illuminating beam calculated using incident beam functions from [4] which uses the point matching method. If it sufficient to terminate the multipole expansion at $n = N_{max}$ where $N_{max} = ka + 3\sqrt[3]{ka}$ [20].

5. Formulating the T -matrix with point matching

Here, we present the point matching method as an alternative to an existing T-matrix method with DDA [13]. The point matching method that we implemented involved matching the fields due to the dipoles with the

fields calculated from vector spherical wave function expansion and at multiple points. The number of points should be such that the linear system of equations are exactly or over determined i.e. the number of equations are the same or greater than the number of unknowns.

Once we have the dipole moments, the \mathbf{E} -field at any point \mathbf{r} (relative to the origin) can be calculated by adding up the contributions from each dipole using the electric dipole field equation from section 9.2 of [21],

$$\mathbf{E}(k\mathbf{r}) = \frac{1}{4\pi\epsilon_0} \left\{ k^2(\hat{\mathbf{r}} \times \mathbf{p}) \times \hat{\mathbf{r}} \frac{e^{ikr}}{r} + [3\hat{\mathbf{r}}(\hat{\mathbf{r}} \cdot \mathbf{p}) - \mathbf{p}] \left(\frac{1}{r^3} - \frac{ik}{r^2} \right) e^{ikr} \right\}, \quad (15)$$

In the far field, the $1/r^2$ and $1/r^3$ terms can be ignored as their contributions diminish rapidly with distance:

$$\mathbf{E}(k\mathbf{r}) = \frac{1}{4\pi\epsilon_0} \left\{ k^2(\hat{\mathbf{r}} \times \mathbf{p}) \times \hat{\mathbf{r}} \frac{e^{ikr}}{r} \right\}. \quad (16)$$

5.1. Near field point matching

The near field calculated via DDA (15) can be matched to scattered field (22) calculated via the VSWFs at points around the scatterer (figure 5). Since we have the dipole moments, P_j , we can derive a ‘field matrix’, \mathbf{F}_{ij} , derived from (15) such that

$$\mathbf{E}_i^{(DDA)} = \sum_{j=1}^{N_{PM}} \mathbf{F}_{ij} \mathbf{P}_j, \quad (17)$$

where N_{PM} is the number of point to be matched, j is the index for the dipole, i is the index for the near field point and each element F_{ij} is a 3×3 tensor. Using the vector identity $(\mathbf{a} \times \mathbf{b}) \times \mathbf{c} = \mathbf{b}(\mathbf{a} \cdot \mathbf{c}) - \mathbf{c}(\mathbf{a} \cdot \mathbf{b})$, the cross product terms in (15) become

$$\begin{aligned} (\hat{\mathbf{r}} \times \mathbf{p}) \times \hat{\mathbf{r}} &= \mathbf{p}(\hat{\mathbf{r}} \cdot \hat{\mathbf{r}}) - \hat{\mathbf{r}}(\hat{\mathbf{r}} \cdot \mathbf{p}) \\ &= \mathbf{p} - \hat{\mathbf{r}}(\hat{\mathbf{r}} \cdot \mathbf{p}). \end{aligned} \quad (18)$$

Substituting the result of (18) into (15) we obtain

$$\mathbf{E} = \frac{e^{ikr}}{r} \left[k^2(\hat{\mathbf{r}}\hat{\mathbf{r}} - \mathbf{1}_3) + \frac{(ikr - 1)}{r^2}(3\hat{\mathbf{r}}\hat{\mathbf{r}} - \mathbf{1}_3) \right] \mathbf{p}, \quad (19)$$

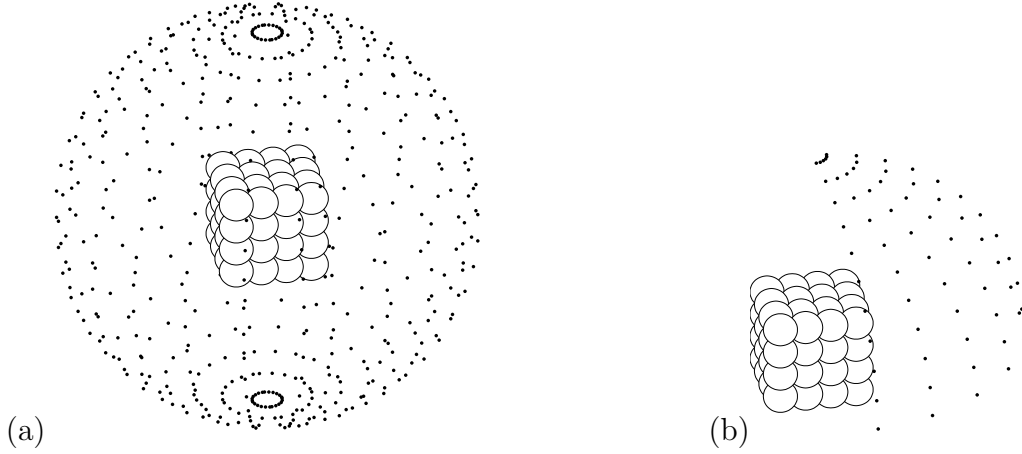


Figure 5: (a) Near field matching and (b) octant near field matching for a dipole model of a cube.

which can also be used to formulate the A-matrix (1). Thus the field matrix in (17) is

$$\mathbf{F}_{ij} = \frac{\exp(ikr_{jk})}{r_{jk}} \left[k^2(\hat{r}_{jk}\hat{r}_{jk} - \mathbf{1}_3) + \frac{ikr_{jk} - 1}{r_{jk}}(3\hat{r}_{jk}\hat{r}_{jk} - \mathbf{1}_3) \right], \quad (20)$$

where \hat{r}_{jk} is the unit vector between a dipole and a matched point. F_{ij} can be precalculated and used when required.

Rotational (5) and mirror (13) symmetry optimizations may also be applied to (17) such that we only need to calculate the fields of the matched points in one octant:

$$\mathbf{E}_i^{(DDA,oct)} = \sum_{j=1}^{N_{PM}/8} \mathbf{F}_{ij}^{(oct)} \mathbf{P}_j^{(oct)}, \quad (21)$$

where only the fields for an octant are calculated (although all the dipole moments are used). This reduces the number of equations by a factor of 64 compared to (17). Now, since the VSWF expansion of the scattered field is

$$\mathbf{E}_{sca} = \sum_{n=1}^{\infty} \sum_{m=-n}^n p_{nm} \mathbf{M}_{nm}^{(1)}(kr) + q_{nm} \mathbf{N}_{nm}^{(1)}(kr). \quad (22)$$

we can solve for the scattering coefficients

$$p_{nm} = \mathbf{M}_{nm}^{(1)}(kr) / \mathbf{E}_{TE,nm}^{(DDA)}, \quad (23)$$

$$q_{nm} = \mathbf{N}_{nm}^{(1)}(kr) / \mathbf{E}_{TM, nm}^{(DDA)}.$$

As we cycle through each combination of n and m , we obtain the solutions for the scattering coefficients p_{nm} and q_{nm} which represent coupling between the n and m incident and scattered modes; p_{nm} and q_{nm} together make up one column of the T -matrix at a time.

5.2. Far field matching

In this method we match the VSWF expansion of the scattered field (22) with that calculated via DDA in far field. We calculate the DDA field in a way similar to (17) but instead, calculating the far field

$$kr \mathbf{E}_i^{(DDA)} = \sum_{i=1}^{N_{PM}} \mathbf{F}_{ij} \mathbf{P}_j, \quad (24)$$

where field matrix, \mathbf{F}_{ij} , from (20) is multiplied by kr and with the latter term omitted to give

$$\mathbf{F}_{ij} = \exp(ikr_{jk}) k^3 (\hat{r}_{jk} \hat{r}_{jk} - \mathbf{1}_3). \quad (25)$$

Now the VSWFs in the expansion of the scattered field (22) are

$$\mathbf{M}_{nm}^{(1)}(kr) = \mathbf{N}_n h_n^{(1)}(kr) \mathbf{C}_{nm}(\theta, \phi), \quad (26)$$

$$\begin{aligned} \mathbf{N}_{nm}^{(1)}(kr) = & \frac{h_n^{(1)}(kr)}{kr N_n} \mathbf{P}_{nm}(\theta, \phi) + \\ & N_n \left(h_{n-1}^{(1)}(kr) - \frac{nh_n^{(1)}(kr)}{kr} \right) \mathbf{B}_{nm}(\theta, \phi) \end{aligned} \quad (27)$$

where $N_n = 1/\sqrt{n(n+1)}$, $h^{(1,2)}$ are spherical Hankel functions and \mathbf{B}_{nm} , \mathbf{C}_{nm} & \mathbf{P}_{nm} are vector spherical harmonics:

$$\begin{aligned} \mathbf{B}_{nm}(\theta, \phi) &= r \nabla \gamma_n^m(\theta, \phi) \\ &= \nabla \times \mathbf{C}_m^n(\theta, \phi) \\ &= \hat{\theta} \frac{\partial}{\partial \theta} \gamma_n^m(\theta, \phi) + \hat{\phi} \frac{im}{\sin \theta} \gamma_n^m(\theta, \phi), \end{aligned} \quad (28)$$

$$\begin{aligned}
\mathbf{C}_{nm}(\theta, \phi) &= \nabla \times (r\gamma_n^m \theta, \phi) \\
&= \hat{\theta} \frac{im}{\sin \theta} \gamma_n^m(\theta, \phi) - \hat{\phi} \frac{\partial}{\partial \theta} \gamma_n^m(\theta, \phi),
\end{aligned} \tag{29}$$

$$\mathbf{P}_{nm}(\theta, \phi) = \hat{r} \gamma_n^m(\theta, \phi) \tag{30}$$

where $\gamma_n^m(\theta, \phi)$ is the normalised scalar spherical harmonics. $\mathbf{M}_{nm}^{(1)}$ and $\mathbf{N}_{nm}^{(1)}$ are the TE and TM multipole fields respectively. In the farfield limit [22, 19] the VSWFs (26) & (27) become

$$\mathbf{M}_{nm}^{(1)}(kr) = \frac{N_n}{kr} (-i)^{n+1} \exp(ikr) \mathbf{C}_{nm}(\theta, \phi) \tag{31}$$

$$\mathbf{N}_{nm}^{(1)}(kr) = \frac{N_n}{kr} (-i)^{n+1} \exp(ikr) \mathbf{B}_{nm}(\theta, \phi). \tag{32}$$

The scattered can be further simplified since $\lim_{r \rightarrow \infty} \exp(ikr) \rightarrow 1$,

$$\mathbf{M}_{nm}^{(1)}(kr) = \frac{N_n}{kr} (-i)^{n+1} \mathbf{C}_{nm}(\theta, \phi) \tag{33}$$

$$\mathbf{N}_{nm}^{(1)}(kr) = \frac{N_n}{kr} (-i)^{n+1} \mathbf{B}_{nm}(\theta, \phi), \tag{34}$$

Now the far field can also be calculated using

$$kr\mathbf{E}(\theta, \phi) = \sum_{nm} b_{nm} \mathbf{B}_{nm} + c_{nm} \mathbf{C}_{nm} + a_{nm} \mathbf{P}_{nm}, \tag{35}$$

where the coefficients b_{nm} & c_{nm} can be calculated (trapezoidal integration) using

$$b_{nm} = \frac{\int kr\mathbf{E} \cdot \mathbf{B}_{nm} d\sigma}{\int \mathbf{B}_{nm} \cdot \mathbf{B}_{nm} d\sigma}, \tag{36}$$

$$c_{nm} = \frac{\int kr\mathbf{E} \cdot \mathbf{C}_{nm} d\sigma}{\int \mathbf{C}_{nm} \cdot \mathbf{C}_{nm} d\sigma}, \tag{37}$$

where $kr\mathbf{E}$ is calculated via DDA; this is where the point matching occurs. The last term in (35) can be ignored because the radial component (30) is negligible in the far field. If we then match the terms in (22), (35) & (33) the scattering coefficients can be determined:

$$p_{nm} = \frac{b_{nm}}{N_n (-i)^{n+1}}, \tag{38}$$

$$q_{nm} = \frac{a_{nm}}{N_n(\mathbf{i})^n}. \quad (39)$$

So, as with the near field matching, we cycle through the n and m modes and insert p_{nm} vertically concatenated with q_{nm} into the appropriate column of the T -matrix for the given mode.

6. Mode redundancy and the order of discrete rotational symmetry

We can also exploit the azimuthal dependence of $\exp(im\phi)$ of each individual VSWF. The discrete rotational symmetry effectively provides a periodic boundary condition, determining the periodicity with respect to the azimuthal angle ϕ . According to Floquet's theorem [23], in the case of the plane wave diffracting from a periodic grating, the wave vectors of the scattered modes are

$$k_{scat} = k_{inc} + ip, \quad i = \dots - 2, -1, 0, 1, 2, \dots \quad (40)$$

where p is the order of discrete rotational symmetry of the scatterer. The spherical wave equivalent is such that the azimuthal modes of the scattered light that couple to a given incident mode is

$$m_{scat} = m_{inc} + ip, \quad i = \dots - 2, -1, 0, 1, 2, \dots \quad (41)$$

For a structure with four-fold discrete rotational symmetry, $p = 4$, thus $m_{sca} = m_{inc}, m_{inc} \pm 4, m_{inc} \pm 8, \dots$. The number of unknowns in the linear system is reduced by a factor of 4. The calculation time saving for this scheme is about 2 to 3 orders of magnitude.

7. Mode-reduced T-matrix

This scheme may be deemed in breach of the true purpose of the T -matrix i.e. it should be good for any illumination at the wavelength for which it was formulated. However, if we know that the only beam that we are going to use is, say the LG_{02} and that the scatterer e.g. figure 1a only spins along the beam axis, and stays on the beam axis, then the only relevant scattering modes when calculating the T -matrix would be $m = 1, 3$.

Bearing in mind that we 'move' the scatterer along the beam axis to find the equilibrium position by calculating the axial force [4]; we perform repeated calculations with the mode-reduced T -matrix without sacrificing any accuracy. Formulating the mode-reduced T -matrix, in most cases, takes a fraction of the time taken for the full-mode T -matrix.

8. Results

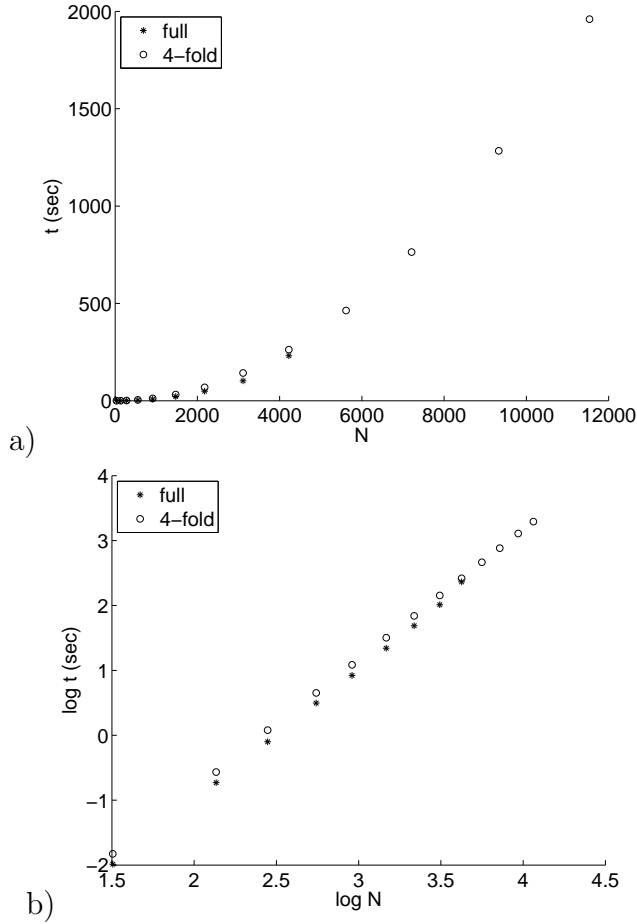


Figure 6: a) Linear and b) log-log plots of the time required to assemble the interaction matrices for versus the number of dipoles (or equivalent for the 4-fold discrete rotational symmetric methodology)

8.1. Symmetry optimization

The rotational symmetry optimized DDA scheme produces results that are no different (well below round-off errors) to that of the standard DDA implementation; there is no appreciable difference that would be visible when plotting comparison data for say the phase function or the extinction. Instead, we present comparison test results for the calculation times for con-

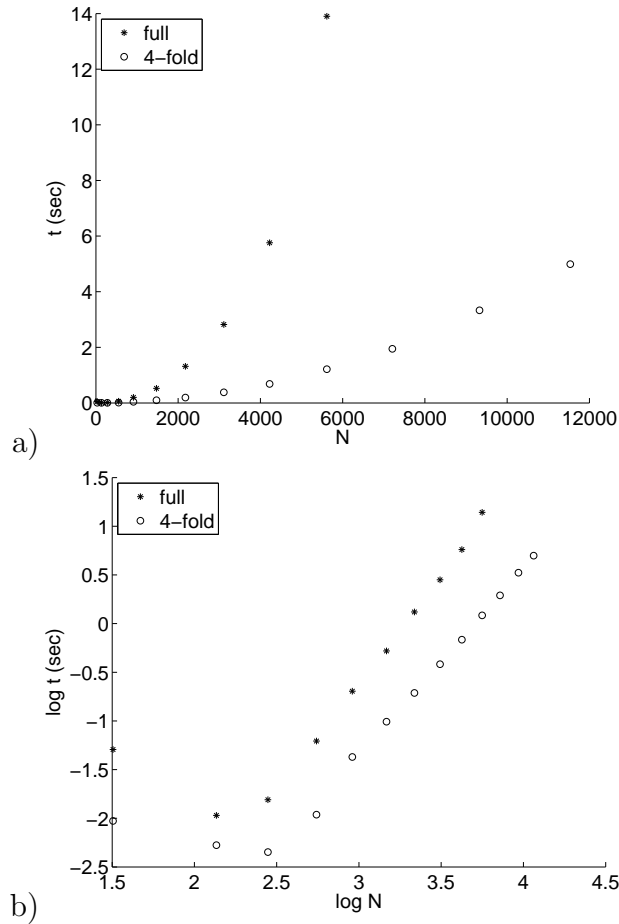


Figure 7: a)Linear and b)log-log plots of the time required to solve for the dipole moments versus the number of dipoles

structuring the A-matrix and for solving the linear equations to obtain the dipole moments.

Note that the full equivalent number of dipoles are plotted (figures 6 & 7) for the case of the rotational symmetric algorithm and not just the number of dipoles in the quadrant.

Although the size of the 4-fold rotationally symmetric interaction matrices are 1/16th that of the conventional interaction matrix, the times required to assemble are comparable (figure 6) and even slightly more for the former because the algorithms (1) & (2) still requires each component of the rotational counterpart in each quadrant to be calculated, including the transformation

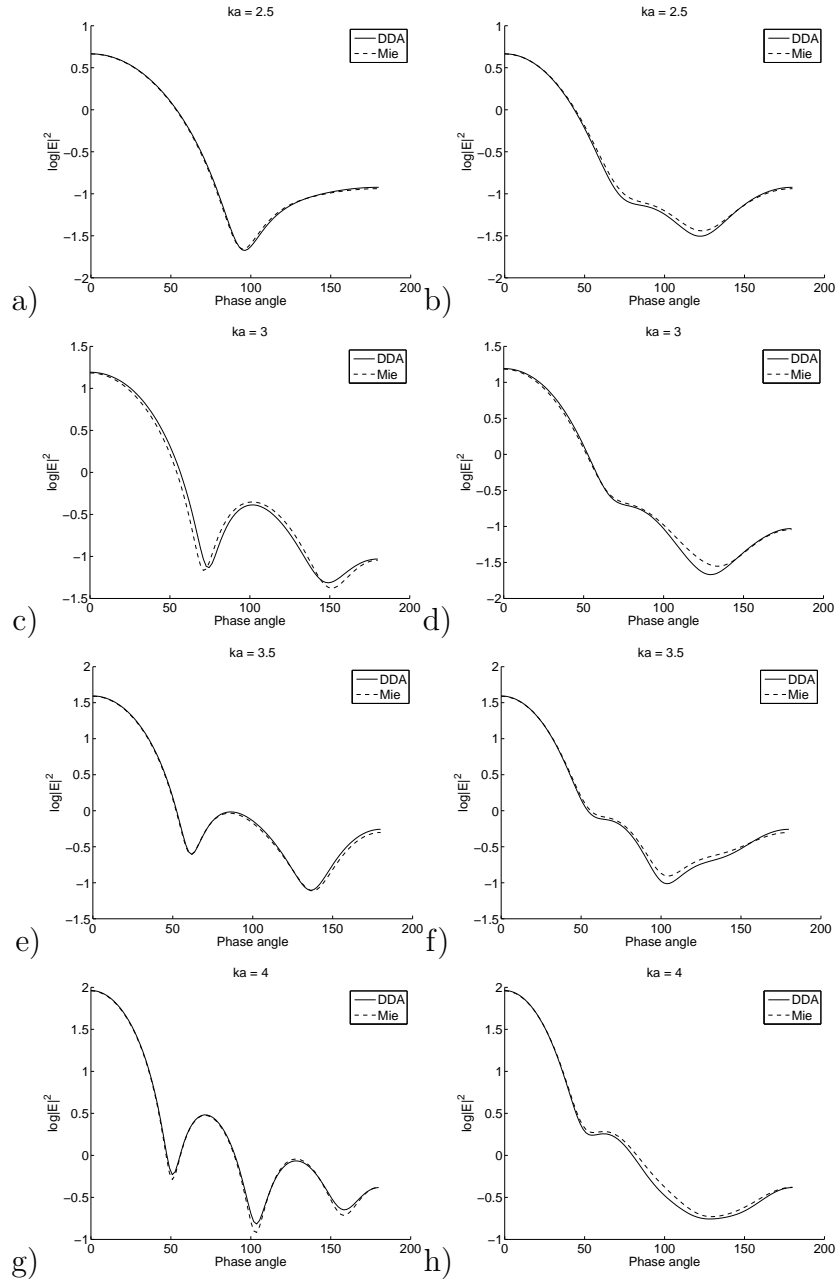


Figure 8: The phase function plots on the left column are for the plane perpendicular to the $(\mathbf{E}$ -field) polarization of the incident plane wave whereas those on the right column are for the parallel plane. The plots for varying size parameters (2.5, 3, 3.5 & 4) are from top to bottom. The relative refractive index is 1.33.

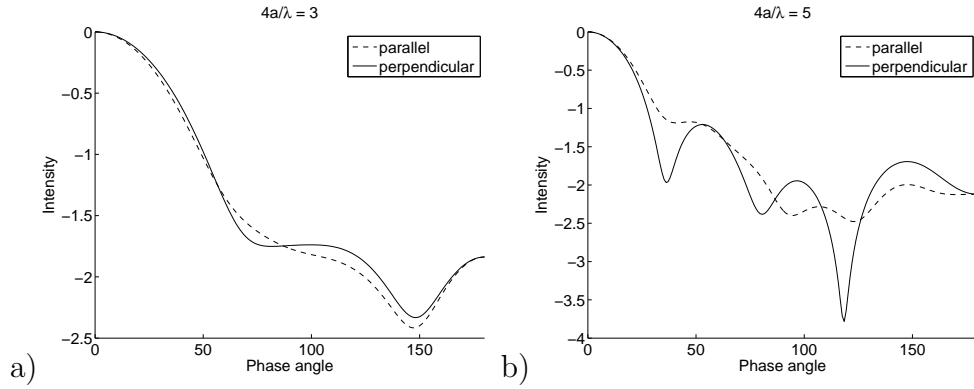


Figure 9: The phase function for cubes with the refractive index of 1.5 and widths of a) 0.75λ b) 1.25λ .

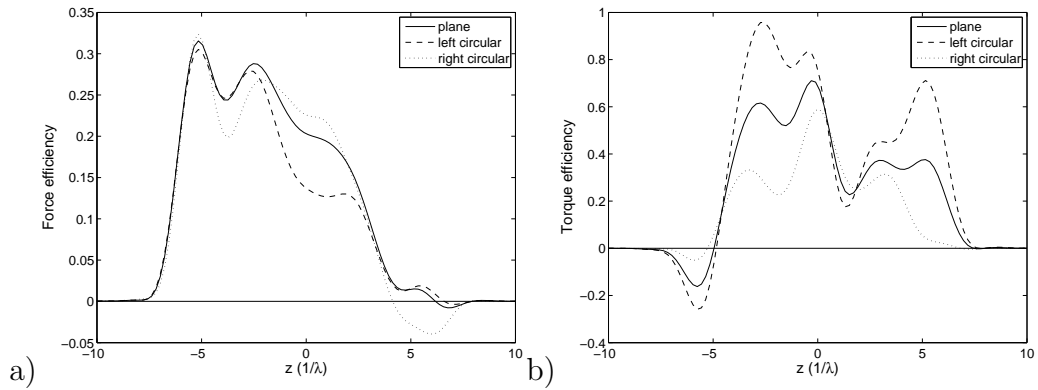


Figure 10: The axial a) force and b) torque as a function of the displacement along the beam axis for an LG_{02} beam with a 71.55° convergence angle, for plane and circular polarisations.

matrices (7 & 6) for changing coordinate systems back and forth. Moreover, the rotationally symmetric A-matrices are azimuthal mode, m , dependent and thus requires $2N_{max} + 1$ number of compressed T -matrices; this number can be reduced by exploiting $\mathbf{A}(m) = \mathbf{A}(-m)$ for m even.

The important advantage is that the memory footprint of the 4-fold discrete rotational symmetry optimized interaction matrix is 1/16th that of its conventional counterpart. For the full interaction matrix, we encountered the problem of disk swapping on a PC with 4Gb of RAM just with > 5000 dipoles and as can be seen on figure 6, we stopped short at < 5000 dipoles because the time taken increased sharply as available memory became scarce. By contrast, the symmetry optimized interaction matrix did not encounter such problems for the range of number of dipoles we tested with.

The reduction (1/16th) of the number of linear equations when calculating the dipole moments results in very significant time savings (figure 7). The comparison of the respective scaling with the number of dipoles can be determined from the gradients of the log-log plot in figure 7b.

8.2. Phase functions for the spheres and cubes

To test the integrity of the optimization methods and the T-matrix via point matching, we compare against the results of the GLMT functions for the sphere [24] and cube [25]. The phase functions in figure 8 were generated from the scattering coefficients obtained from the T-matrices; the results show good agreement against the Mie solution, allowing for stair casing errors when trying to approximate a sphere with a cubic lattice arrangement of dipoles with finite lattice spacing.

The rotational symmetry algorithm was tested for cubes, since they possess 4-fold rotational symmetry and analytical results can be calculated. The T-matrix via point matching was also applied and the results (figure 8) compared favourably against those produced from the GLMT method in [25].

8.3. Cross rotor torque calculations

All the optimization methods and the point matching method for formulating the T-matrix were applied to calculating the forces and torques imparted on the microrotor (figure 1a) by a tightly focused and trapping LG_{02} laser beam. We were able to determine the axial equilibrium position (figure 8a) i.e. the point at which the axial force curve crosses the z-axis with negative gradient. The torque varies dramatically as we move along the beam axis but we are only interested in the torque at equilibrium. There are

a number of uncertainties in experimental measurement that we endeavour to narrow down but the results between the model and experiment agree within the error limits.

9. Discussion

The rotational and mirror symmetry algorithms do not introduce any errors (well below round-off errors) to the DDA calculation. The construction of the interaction matrix takes a large portion of the calculation time for the DDA method in general; in principle, the compressed interaction matrix offers no advantage here. Because the compressed interaction matrix is azimuthal mode dependent, it can be cumbersome when formulating the T-matrix; we load the precalculated matrices as required. However, there are two major advantages of the symmetry optimization scheme. Firstly, their memory footprint is significantly smaller; we are otherwise unable to model our microrrotors, given their size, on desktop PCs. Secondly, the time savings when calculating the dipole moments more than make up for the extra time spent for the compressed interaction matrices.

The mode redundancy algorithms give further time savings of about two orders of magnitude, as with the mode-reduced T-matrices where applicable.

There are a number of factors that contribute to errors and uncertainties between the quantities of interest between experimental and modelling results. In our DDA model, we assume that the material is linear and non-absorbing. The lattice spacing is finite, which leads to stair casing errors and an inaccurate representation of the target. The characteristics of the driving beam does invariably differ to some degree compare to that of the intended beam due to imperfections in the optical setup. Taking all these factors into consideration, the methods in described in this paper gives us sufficient accuracy in modelling light scattering from the micromachines that we continue to design and develop.

References

- [1] A. Ashkin, J. M. Dziedzic, J. E. Bjorkholm, S. Chu, Observation of a single-beam gradient force optical trap for dielectric particles, *Opt. Lett.* 11 (1986) 288–290.
- [2] D. G. Grier, A revolution in optical manipulation, *Nature* 424 (6950) (2003) 810–816.
- [3] T. A. Nieminen, S. Parkin, T. Asavei, V. L. Y. Loke, H. N. R., H. Rubinsztein-Dunlop, Optical vortex trapping and the dynamics of particle rotation, in: D. L. Andrews (Ed.), *Structured Light and Its Applications: An Introduction to Phase-Structured Beams and Nanoscale Optical Forces*, Academic Press, San Diego, 2008, pp. 195–236.
- [4] T. A. Nieminen, V. L. Y. Loke, A. B. Stilgoe, G. Knöner, A. M. Bracúzyk, N. R. Heckenberg, H. Rubinsztein-Dunlop, Optical tweezers computational toolbox, *J. Opt. A* 9 (2007) S196–S203.
- [5] V. L. Y. Loke, T. A. Nieminen, S. W. Parkin, N. R. Heckenberg, H. Rubinsztein-Dunlop, Fdfd/t-matrix hybrid method, *JQSRT* 106 (2007) 274–284.
- [6] E. Purcell, C. Pennypacker, Scattering and absorption of light by non-spherical dielectric grains, *Astrophys. J.* 186 (1973) 705–714.
- [7] B. T. Draine, P. J. Flatau, Discrete-dipole approximation for scattering calculations, *J. Opt. Soc. Am. A* 11 (4) (1994) 1491–1499.
- [8] P. C. Waterman, Matrix formulation of electromagnetic scattering, *Proc. IEEE* 53 (1965) 805–812.
- [9] P. C. Waterman, Symmetry, unitarity, and geometry in electromagnetic scattering, *Phys. Rev. D* 3 (4) (1971) 825–839.
- [10] M. Mishchenko, L. Travis, A. Lacis, *Scattering, Absorption, and Emission of Light by Small Particles*, Cambridge University Press, Cambridge, 2002.
- [11] T. Asavei, S. Parkin, M. Persson, R. Vogel, M. Funk, V. L. Y. Loke, T. A. Nieminen, H. Rubinsztein-Dunlop, N. R. Heckenberg, Engineering optically driven micromachines, *Proc. SPIE* 7038 (2008) 03816.

- [12] T. Asavei, T. A. Nieminen, N. R. Heckenberg, H. Rubinsztein-Dunlop, Fabrication of micro-structures for optically driven micromachines using two-photon photopolymerization, to appear in *J. of Opt. A* (2009).
URL <http://arxiv.org/pdf/0810.5585>
- [13] D. W. Mackowski, Discrete dipole moment method for calculation of the T-matrix for nonspherical particles, *J. Opt. Soc. Am. A* 19 (5) (2002) 881–893.
- [14] W. L. Collett, C. A. Ventrice, S. M. Mahajan, Electromagnetic wave technique to determine radiation torque on micromachines driven by light, *Appl. Phys. Lett.* 82 (16) (2003) 2730–2732.
- [15] B. T. Draine, J. Goodman, Beyond clausius-mossotti: wave propagation on a polarizable point lattice and the discrete dipole approximation, *Astrophys. J.* 405 (1993) 685–697.
- [16] Y. Saad, M. H. Schultz, Gmres: a generalized minimal residual method for solving nonsymmetric linear systems, *SIAM J. Sci. Stat. Comput* 7 (1986) 856–869.
- [17] T. A. Nieminen, N. R. Heckenberg, H. Rubinsztein-Dunlop, Calculation of the T-matrix: general considerations and application of the point-matching method, *JQSRT* 79-80 (2003) 1019–1029.
- [18] M. I. Mischenko, J. W. Hovenier, L. D. Travis, Light scattering by nonspherical particles: theory, measurements and applications, Academic Press, San Diego, 2000.
- [19] T. A. Nieminen, N. R. Heckenberg, H. Rubinsztein-Dunlop, Multipole expansion of strongly focussed laser beams, *JQSRT* 79-80 (2003) 1005–1017.
- [20] B. Brock, Using vector spherical harmonics to compute antenna mutual impedance from measured or computed fields, Tech. Rep. SAND2000-2217-Revised, Sandia National Laboratories, Albuquerque, NM, (unpublished) (2001).
- [21] J. D. Jackson, *Classical Electrodynamics*, Wiley, New York, 1998, 3rd ed.

- [22] M. I. Mishchenko, Light-scattering by randomly oriented axially symmetrical particles, *J. Opt. Soc. Am. A* 8 (6) (1991) 871–882.
- [23] P. S. J. Russell, Coupled wave versus modal theory in uniform dielectric gratings, *Opt. Commun.* 48 (1983) 71–74.
- [24] H. C. van de Hulst, *Light scattering by small particles*, Wiley, New York & London, 1957.
- [25] T. Wriedt, U. Comberg, Comparison of computational scattering methods, *JQSRT* 60 (3) (1998) 411–423.